# Supplementary information

# Gas phase deposition of well-defined bimetallic gold-silver clusters for photocatalytic applications

Vana Chinnappa Chinnabathini[a,b,c], Fons Dingenen[b,c], Rituraj Borah[b,c], Imran Abbas[a], Johan van der Tol[a], Zviadi Zarkua[a], Francesco D'Acapito[d], Thi Hong Trang Nguyen[a], Peter Lievens[a], Didier Grandjean[a], Sammy W. Verbruggen[b,c], Ewald Janssens[a]

*a Quantum Solid-State Physics, Department of Physics and Astronomy, KU Leuven, Belgium*
*b Sustainable Energy, Air & Water Technology (DuEL), University of Antwerp, Belgium*
*c NANOlab Center of Excellence, University of Antwerpen, Groenenborgerlaan 171, 2020, Antwerpen, Belgium*
*d. CNR-IOM-OGG c/o ESRF LISA CRG - The European Synchrotron, Grenoble, France.*

Emails to: chinnabathini.vanachinnappa@kuleuven.be, ewald.janssens@kuleuven.be and didier.grandjean@kuleuven.be

**Supplementary information contains:**

- **Table S1.** Structural results of Au $L_3$-edge EXAFS refinements
- **Figure S1.** Size distribution of $Au_xAg_{1-x}$ clusters measured by time-of-flight mass spectrometry
- **Figure S2.** SEM images of pure $TiO_2$ and $Au_xAg_{1-x}$ (x= 1, 0.9, 0.7, 0.5, 0.3, 0.1 and 0) cluster-modified $TiO_2$ P25
- **Figure S3**. SEM images of $Au_{0.3}Ag_{0.7}$ on $TiO_2$ P25 for different cluster loadings
- **Figure S4.** XPS survey spectra for $Au_xAg_{1-x}$ clusters on $TiO_2$
- **Figure S5.** O 1s, Ag 3d and Au 4f XPS spectra of $Au_xAg_{1-x}$ bimetallic clusters on $TiO_2$
- **Figure S6.** XPS Integrated peak area of C 1s and Ti 2p peak positions
- **Figure S7**. Comparison of Ag $3d_{3/2}$ and Au $4f_{5/2}$ BE of $Au_xAg_{1-x}$ bimetallic clusters deposited on $TiO_2$ and their counterparts deposited on $SiO_2$
- **Figure S8.** FQE under UV and solar simulator as a function of cluster coverage
- **Figure S9.** Near-field enhancement maps of isolated nanoparticles of different compositions
- **Figure S10**. $k^2$ weighted XAFS spectra of the $Au_xAg_{1-x}$ bimetallic clusters on $TiO_2$ and carbon supports

# Table

**Table S1.** Summary of structural results of Au $L_3$-edge EXAFS refinements of the $Au_xAg_{1-x}$ clusters

| **Sample** | **$Au_{0.1}Ag_{0.9}$** | **$Au_{0.3}Ag_{0.7}$** | **$Au_{0.5}Ag_{0.5}$** | **$Au_{0.7}Ag_{0.3}$** | **$Au_{0.9}Ag_{0.1}$** |
|---|---|---|---|---|---|
| **Support** | $TiO_2$ | Carbon | Carbon | Carbon | $TiO_2$ |
| **$E_f$ (eV)** | -8.6 (9) | -7.7 (6) | -7.7 (8) | -7.9 (8) | -8.2 (8) |
| **AFAC** | 0.8 | 0.8 | 0.8 | 0.8 | 0.8 |
| **k-range ($A^{\circ -1}$)** | 2.8-11 | 2.8-11.5 | 2.8-11.5 | 2.8-11.5 | 2.8-10 |
| **$N_{Ag}$** | 10.0 (9) | 8.3 (6) | 5.6 (8) | 3.0 (5) | 1.0 (2) |
| **$R_{Ag}$ ($A^{\circ}$)** | 2.86 (3) | 2.85 (1) | 2.85 (2) | 2.84 (3) | 2.82 (5) |
| **$A_{Ag}$ ($Å^2$)** | 0.027 (3) | 0.021 (2) | 0.021 (4) | 0.017 (4) | 0.03 (4) |
| **$N_{Au}$** | 1.0 (3) | 2.9 (4) | 5.5 (8) | 8.0 (9) | 10.0 (9) |
| **$R_{Au}$ ($A^{\circ}$)** | 2.87 (9) | 2.86 (1) | 2.85 (2) | 2.87 (1) | 2.87 (1) |
| **$A_{Au}$ ($Å^2$)** | 0.02 (1) | 0.015 (2) | 0.016 (4) | 0.018 (3) | 0.019 (3) |
| **$N_{Ag}$+ $N_{Au}$** | 11 | 11.2 | 11.1 | 11 | 11 |
| **Diameter (nm)** | ~5 | ~5 | ~5 | ~5 | ~5 |
| **$N_{Au}$/ $N_{Ag}$+ $N_{Au}$** | 0.09 | 0.26 | 0.50 | 0.72 | 0.91 |
| **R (%)** | 42% | 34% | 45% | 46% | 41% |

**$E_f$** = contribution of the wave vector of the zero photoelectron relative to the origin of k

**AFAC** (amplitude reduction due to many-electron processes) was set to 0.8.

**k**= photoelectron wavenumber

**N** = number of atoms in each shell

**R** = distance between neighboring atoms in each shell

**A** = Debye-Waller term of each shell ($A=2\sigma^2$ with $\sigma$ = Debye-Waller factor) ($Å^2$)

**R factor in %** = percentage fit- Agreement factor

# Figures

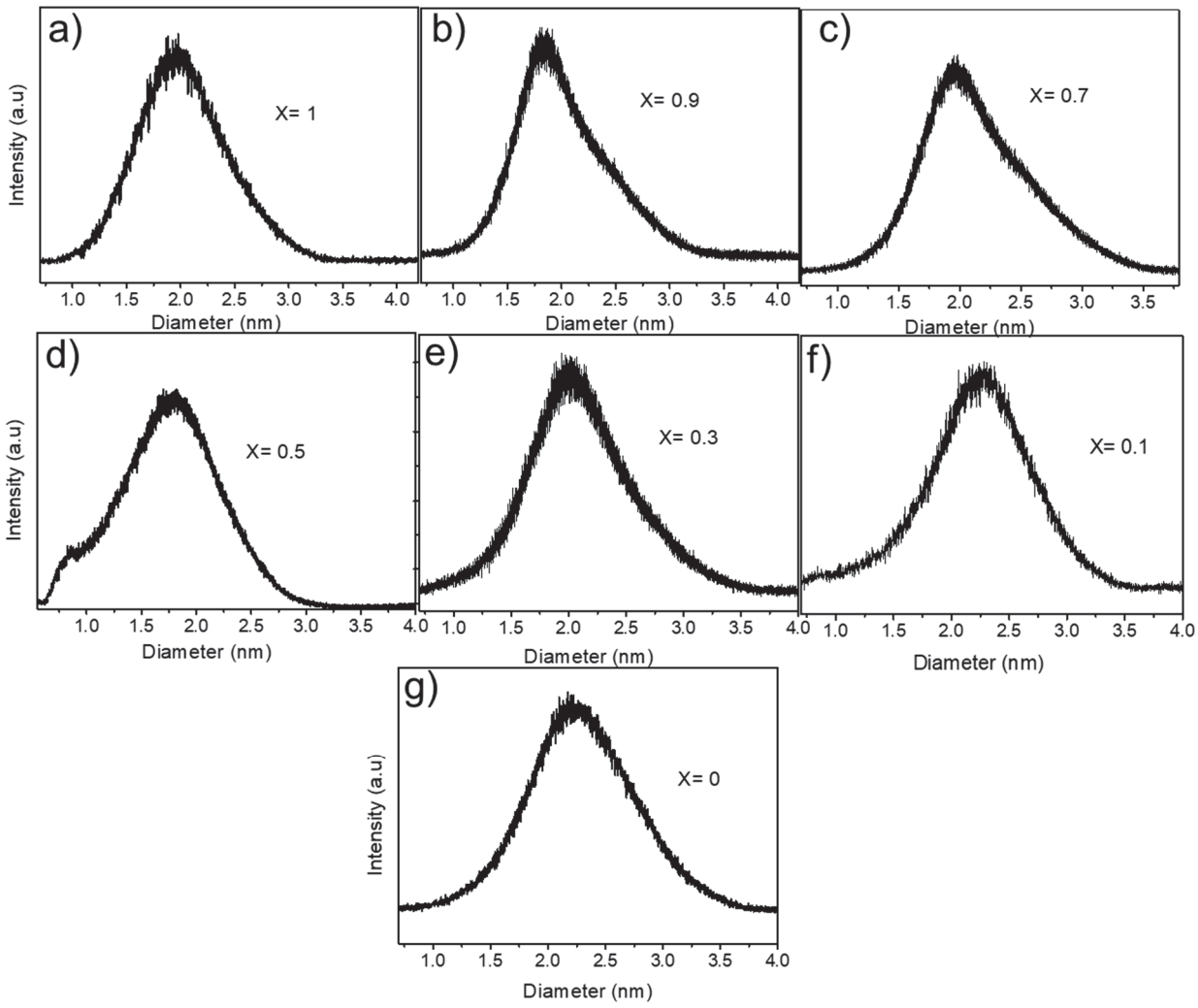


**Figure S1.** Size distribution of $Au_xAg_{1-x}$ (x= 1, 0.9, 0.7, 0.5, 0.3, 0.1 and 0) bimetallic clusters as measured by time-of-flight mass spectrometry prior to cluster deposition. The cluster diameter is deduced from the measured mass assuming a spherical shape and bulk density.

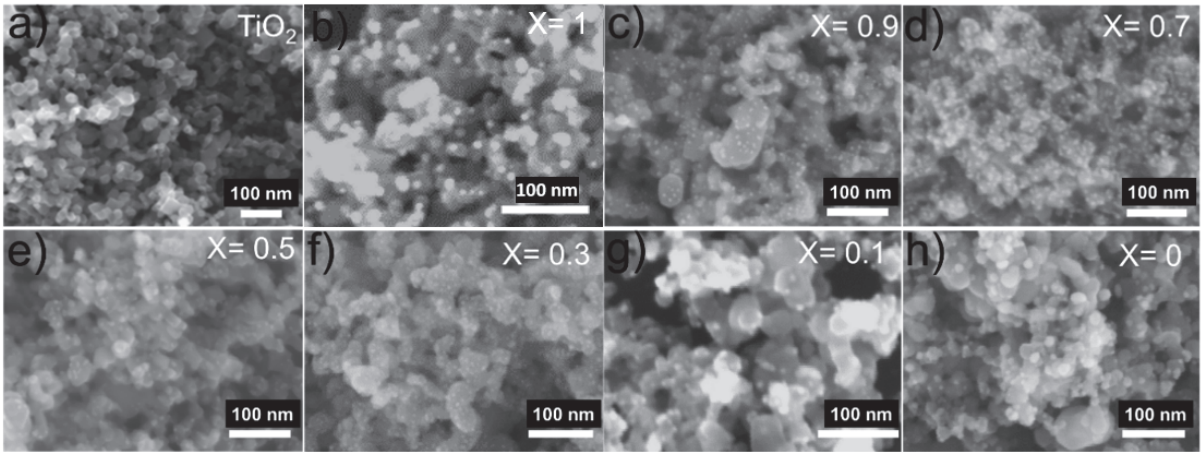


**Figure S2.** SEM images of pure $TiO_2$ and $Au_xAg_{1-x}$ (x= 1, 0.9, 0.7, 0.5, 0.3, 0.1 and 0) cluster-modified $TiO_2$ P25 (small white spots are clusters).

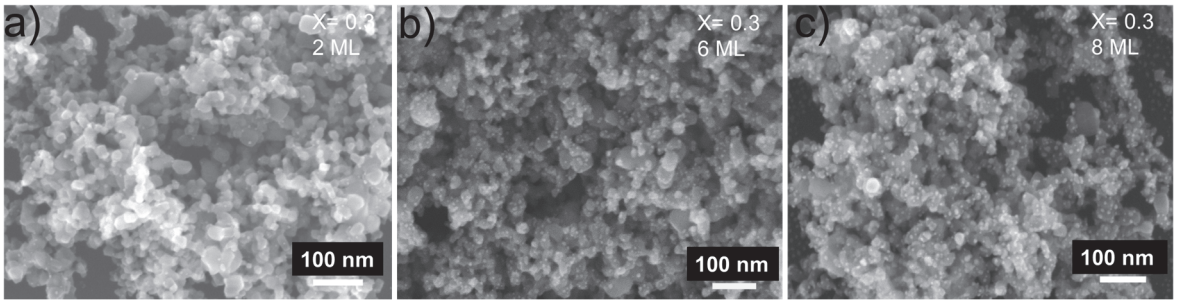


**Figure S3**. SEM images of $Au_{0.3}Ag_{0.7}$ clusters for different loading of 2 ML (a), 6 ML (b), and 8 ML (c). The apparent cluster sizes become larger with the increased loading (see figure 2 in the main manuscript), which indicates cluster coalescence.

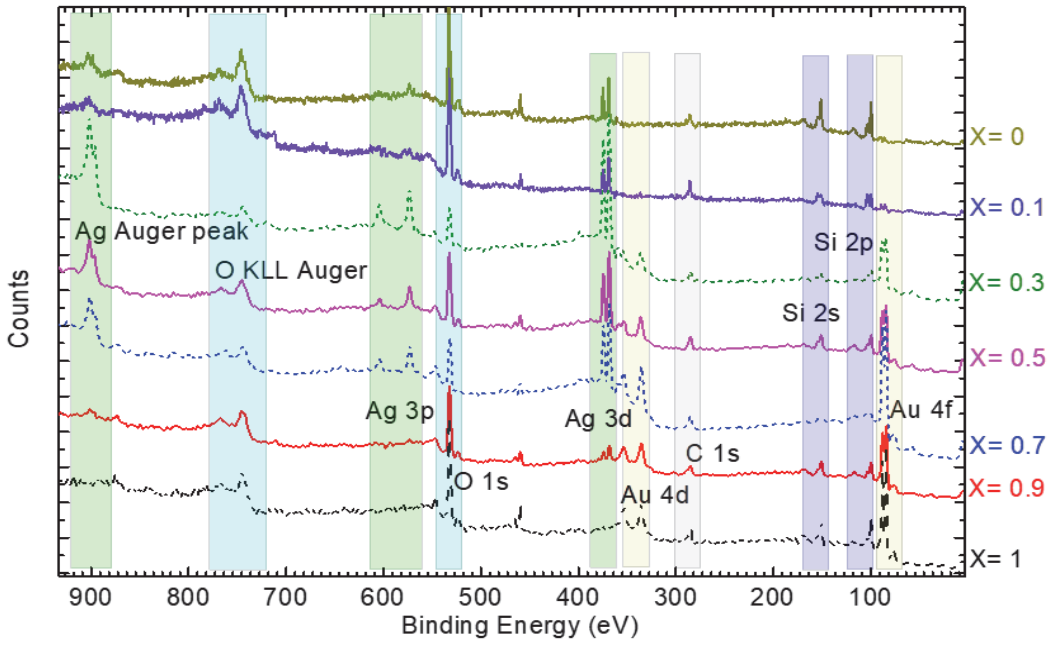


**Figure S4.** XPS survey spectra obtained for $Au_xAg_{1-x}$ (x= 1, 0.9, 0.7, 0.5, 0.3, 0.1, and 0) clusters on $TiO_2$.

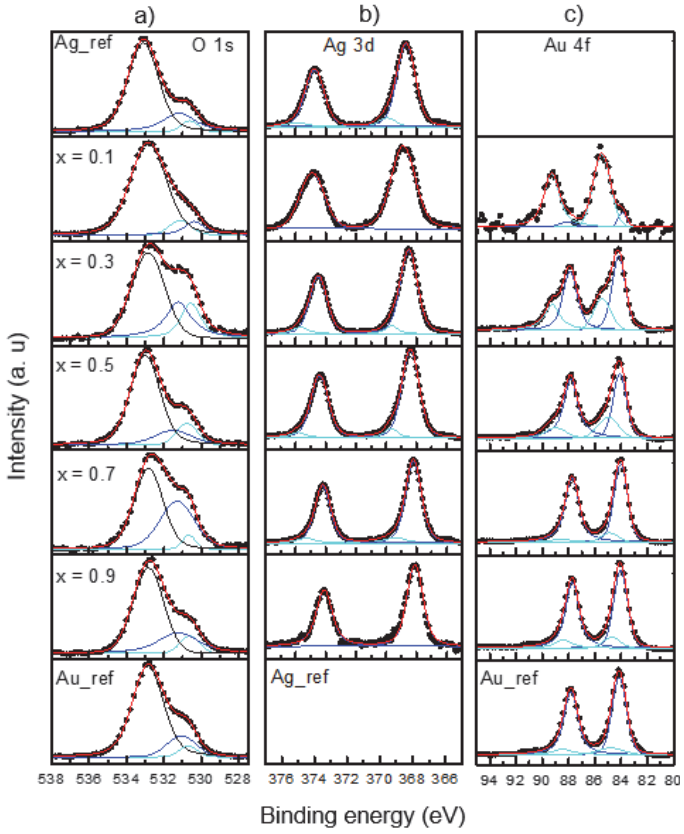


**Figure S5.** (a) O 1s, (b) Ag 3d and (c) Au 4f XPS spectra of the $Au_xAg_{1-x}$ bimetallic clusters on $TiO_2$ from x = 1 to 0

Figure S5 presents the XPS spectra O 1s, Ag 3d, Au 4f of core levels for $Au_xAg_{1-x}$ (X= 1, 0.9, 0.7, 0.5, 0.3, 0.1 and 0) bimetallic clusters deposited on $TiO_2$. The measured data is represented by black dots and the fitting curve by a red line. Shirley step function was used to remove the background and peaks were fitted with Voigt line shapes. From the Ag 3d core level, a shift of peak to higher binding energy (around 0.6 eV) is observed with increasing Ag concentration in the clusters (see Figure 4 in main text). A second Voigt line is added to the fit to accounts for the asymmetric shape of the Ag peak[1]. The Au 4f core level consists of pure Au (blue Voigt line) and alloy Au components[2] (cyan Voigt line), which both shift to higher binding energy with decrease in Au concentration (see Figure 4 in main text).

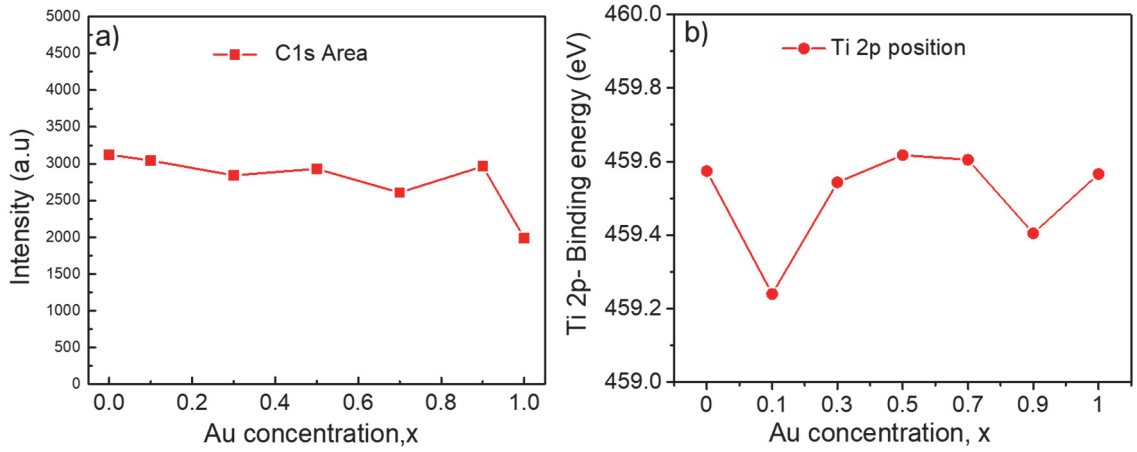


**Figure S6.** a**)**. Integrated peak area of the C 1s level measured through XPS. The value is similar for the different $Au_xAg_{1-x}$ compositions. b). Ti 2p peak position in all studied samples.

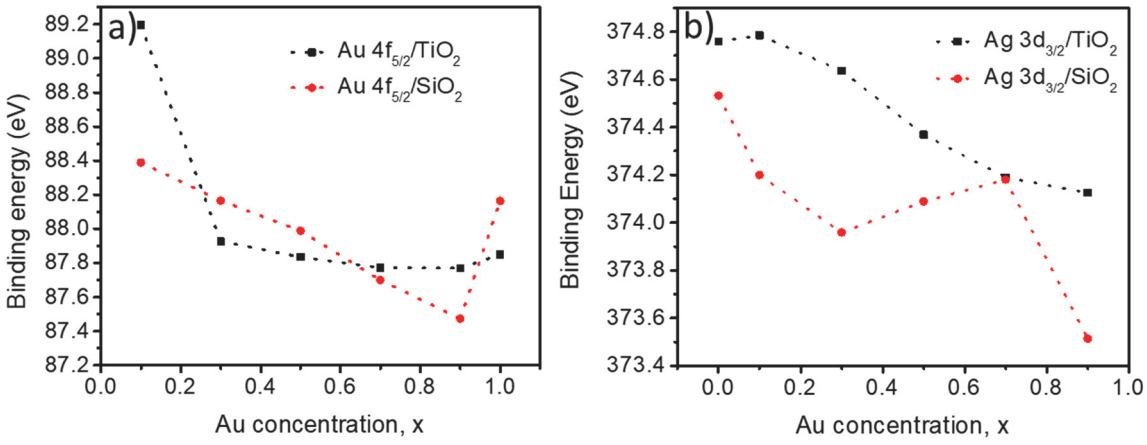


**Figure S7**. Binding energies of Ag 3d $_{3/2}$ and Au 4f $_{5/2}$ states in $Au_xAg_{1-x}$ bimetallic clusters deposited on $TiO_2$ and $SiO_2$. The values for the clusters on $SiO_2$ are taken from ref [3].

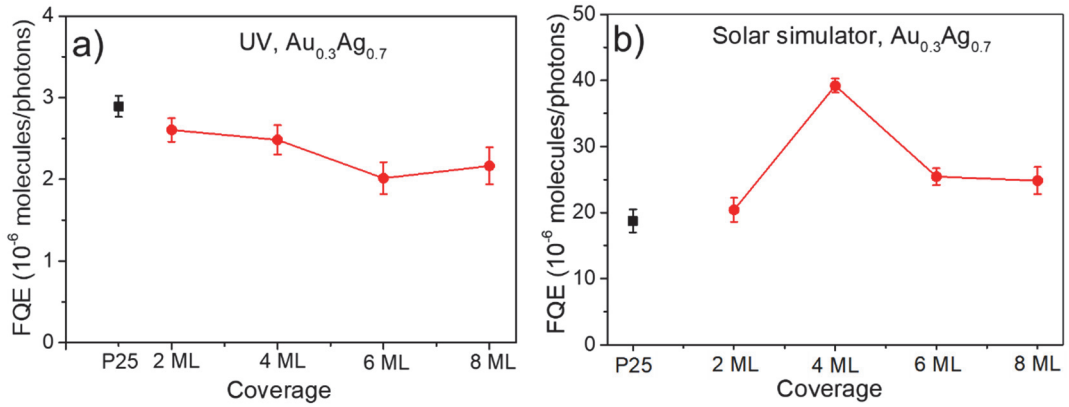


**Figure S8.** FQE under (a) UV and (b) solar simulator as a function of the bimetallic $Au_{0.3}Ag_{0.7}$ cluster coverage.

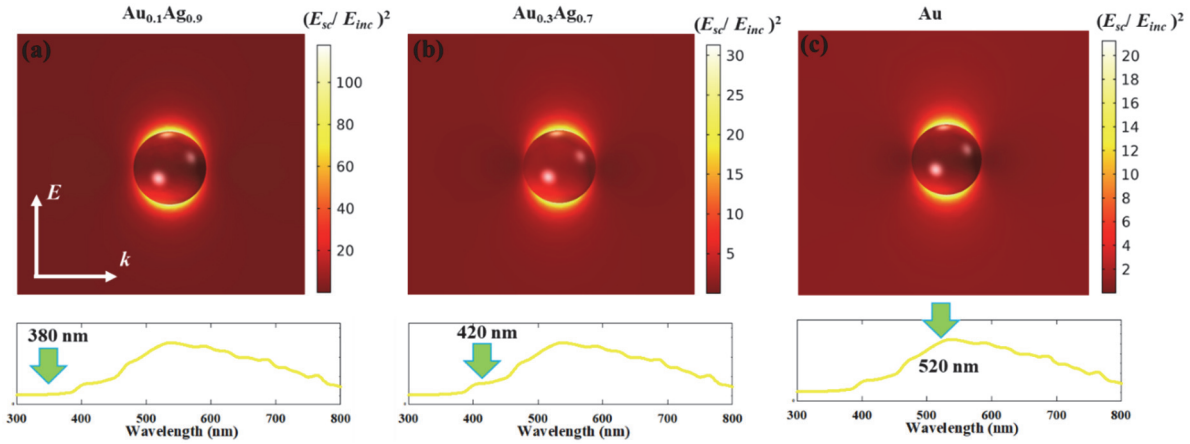


**Figure S9.** Near-field enhancement maps of isolated nanoparticles of three different compositions namely (a) $Au_{0.1}Ag_{0.9}$, (b) $Au_{0.3}Ag_{0.7}$ and (c) Au with the solar light intensity at their LSPR wavelengths 380 nm, 420 nm and 520 nm, respectively. E and k vectors in (a) represent direction of electric field and the light wave, respectively.

These field enhancement maps explain why the $Au_{0.3}Ag_{0.7}$ composition is optimal for the photoactivity. $Au_{0.1}Ag_{0.9}$ has a strong resonance, but at a wavelength where there is basically no intensity in the solar simulator. Pure Au sample has its resonance near the maximum intensity wavelength of solar light, but the overall field enhancement is much lower than that of the Ag-rich particles, and the photon energy is low. The $Au_{0.3}Ag_{0.7}$ sample, has an intermediately strong resonance, centered around the high energy wavelengths of the solar simulator (UV + blue), hence combining a high photon utilization capacity with a strong field enhancement.

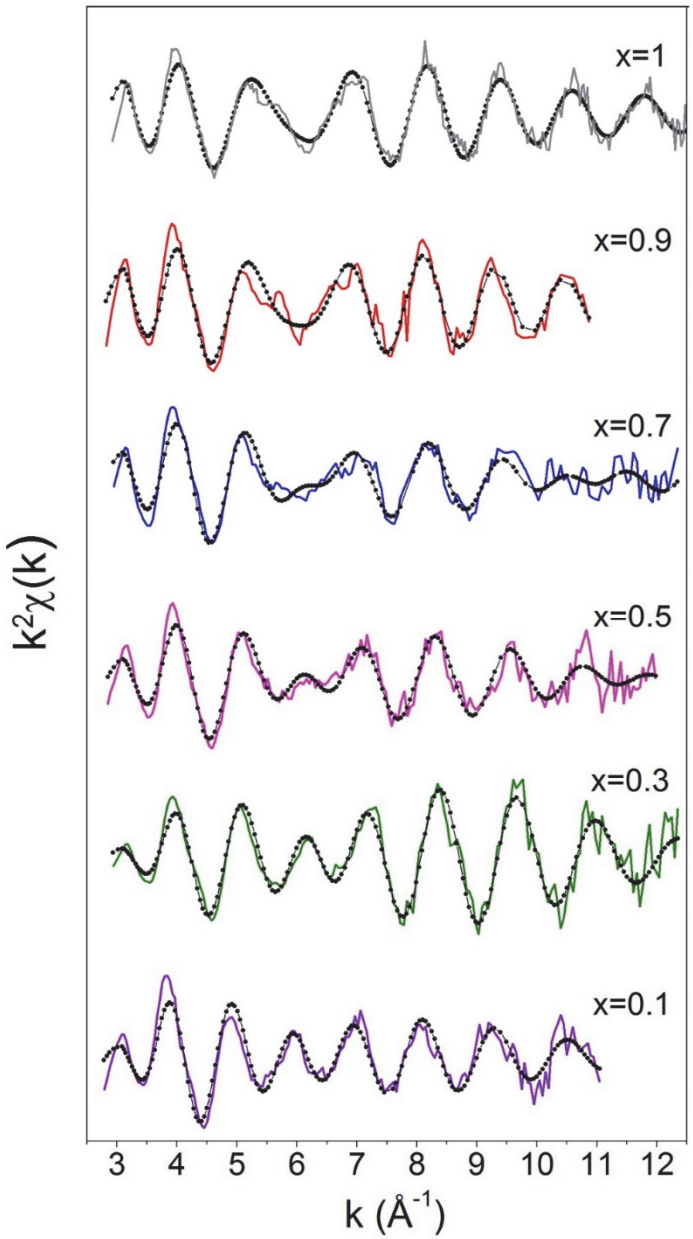


**Figure S10**. $k^2$ weighted XAFS spectra of the $Au_xAg_{1-x}$ bimetallic clusters on $TiO_2$ and carbon supports from x = 1 to 0.1, along with a spectrum from pure Au clusters that is taken from ref. [4]. The corresponding phase-corrected Fourier transformed EXAFS spectra are presented in main text Figure 3.

## References


1. C. D. Wanger, W. M. Riggs, L.E. Davis, J. F. Moulder and G. E, Muilenberg, 1978, *Handbook of X-ray Photoelectron Spectroscopy* (Minnesota: Perkin-Elmer Corporation)
2. P. H. Citrin, G. K. Wertheim and Y. Baer, *Phys. Rev. B*, 1983 vol 27, Issue **6,** 3160-3175.
3. T. W. Liao, A. Yadav, K. J. Hu, J. van der Tol, S. Cosentino, F. D'Acapito, R. E. Palmer, C. Lenardi, R. Ferrando, D. Grandjean and P. Lievens, *Nanoscale*, 2018, **10**, 6684-6694.
4. A. Yadav, Y. Li, T.-W. Liao, K.-J. Hu, J. E. Scheerder, O. V. Safonova, T. Höltzl, E. Janssens, D. Grandjean and P. Lievens, *Small*, 2021, **17**, 2004541.